Osmotic prestressing of a spinal motion segment

Document status and date:
Published: 01/01/1993

Document Version:
Publisher's PDF, also known as Version of Record (includes final page, issue and volume numbers)

Please check the document version of this publication:

• A submitted manuscript is the version of the article upon submission and before peer-review. There can be important differences between the submitted version and the official published version of record. People interested in the research are advised to contact the author for the final version of the publication, or visit the DOI to the publisher's website.
• The final author version and the galley proof are versions of the publication after peer review.
• The final published version features the final layout of the paper including the volume, issue and page numbers.

Link to publication

Download date: 04. Oct. 2023

OSMOTIC PRESTRESSING OF A SPINAL MOTION SEGMENT

Snijders, H., Houben, G.B., Drost, M.R., Huyghe, J.M., Janssen, J.D., Huson A.

Dept. of Movement Sciences, University of Limburg, Maastricht, The Netherlands.
Dept. of Mechanical Engineering, Eindhoven University of Technology, Eindhoven, The Netherlands.

Summary

The mechanical behaviour in axial compression of a human lumbar motion segment (MS) without the facet joints (posterior elements) is modelled using two porous medium descriptions, one including, the other excluding Donnan osmosis. Donnan osmosis is shown to affect the anulus fibre and ground matrix stresses and the fluid flow through the intervertebral disc. Hence, models not including the osmotic effect appear to be inadequate with respect to the prediction of these quantities. In an axial compression simulation of the motion segment major differences occur in axial displacement (after 10 h biphasic 16% more than triphasic), expelled fluid volume versus time (after 10 h triphasic 28% less), fluid pressure (at the base at the inner anulus after 50 s triphasic 26% higher than biphasic), and fibre stress (at the base at the anulus edge after 50 s triphasic 60% higher than biphasic). Although the triphasic simulation maintains a higher fluid pressure, less water is expelled.

Introduction

The human lumbar spine constitutes a mechanical unit that allows for flexion, extension and rotation, while it supports the body. The basic unit of the spine is the motion segment (MS) which consists of 2 vertebrae that enclose the intervertebral disc (IVD). Intervertebral disc tissue consists of a collagen and elastin fibre network embedded in a hydrated proteoglycan (PG) matrix. Small nutrients and ions are dissolved within the tissue. Because of the entanglement of the PG and the fibre network only the interstitial fluid and the small ions can flow. The PG are ionized and because they are relatively stagnant, osmotic effects are important (Urban and Maroudas, 1979).

Mechanical models of the IVD are described in terms of the theory of mixtures. In the biphasic mixture model the solid and fluid phases are regarded as two separate continua. The biphasic model has been used as a basis for finite element modelling of the IVD (Simon et al., 1985). When, however, the osmotic effect plays an important role, it must be accounted for as a third phase: the ionic phase (Lai et al., 1991, Snijders et al., 1992). As the osmotic force is

deformation dependent, it cannot be accounted for in the biphasic model using a constant term. To demonstrate the differences between the bi- and triphasic approaches, we compared the models in an axial compression simulation of a motion segment.

Theory

Deformation of the tissue can be achieved either by mechanical or chemical loading. The overall response is a result of the (1) diffusion of mobile ions, (2) the large deformation of the fibre network and the ground substance with relative fluid flow, and (3) osmosis. In order to describe this complex behaviour we use the theory of mixtures (Bowen, 1980, Müller, 1985). Starting with the kinematic relationships and the general balance laws, specific assumptions for intervertebral disc tissue are incorporated and constitutive restrictions based on the entropy principle are derived (Snijders et al., 1992). The resulting equations are: mass balance (continuity) of the mixture, momentum balance of the mixture and the diffusion equation of the ions. In this study no ion diffusion is used, but simply an instantaneous ion distribution based on Donnan equilibrium for large negatively charged molecules (PG) and small univalent ions. This is admissible because of the constant external ion concentration. Due to the solid deformation ions will still move out of the tissue, but this migration is taken up largely by the convection with water. Hence, diffusion only plays an important role in the <u>local</u> redistribution of ions. The equations are given below:

$$\text{momentum} \quad : \vec{\nabla} \circ \underline{\sigma} - \vec{\nabla} p = \vec{0}$$

$$\text{continuity} \quad : \vec{\nabla} \circ \vec{v}^s - \vec{\nabla} \circ [\underline{K} \circ \vec{\nabla}(p - \varpi)] = 0 \qquad (1)$$

$$\text{ion distribution} : 2c^- = -c^{pg} + \sqrt{(c^{pg})^2 + 4c^2}$$

$$\text{osmosis} \quad : \varpi = \chi(2c^- + c^{pg})$$

with
$\underline{\sigma}$ the solid Cauchy stress tensor
p the hydrodynamic pressure
$\vec{v}^s$ the velocity of the solid
$\underline{K}$ the permeability tensor

c^- the anion concentration
c the external salt concentration
c^{pg} the proteoglycan concentration
χ the osmotic coefficient

The primary unknowns are the displacement of the solid $\vec{u}$, the fluid pressure p and the ion concentration c^-. The equations above, combined with the appropriate material behaviour, initial and boundary conditions complete the description of the mechanical behaviour of intervertebral disc tissue. To solve this problem the Finite Element Method is used (Snijders et al, in press). A Total Lagrange (Newton-Raphson iteration scheme, Houbolt third order time integration scheme) formulation based on the Galerkin method is implemented in the commercial FE-package DIANA (DIANA Analysis B.V., Delft, the Netherlands). For the numerical studies iso-parametric elements of the serendipity family are used. Two dimensional (plane strain and plane stress), three dimensional and axisymmetric elements have been developed. The interpolation functions are the same for displacements, pressures and concentrations and can be either linear or parabolic.

Geometry

For an axial compression load less than 1000 N the facet joints do not contribute significantly to the load transmission (Adams and Hutton, 1980). As the load which is used in the calculations is 650 N maximum the posterior elements are neglected. For the sake of simplicity the remaining disc and vertebra are approximated by an axi-symmetrical geometry. In fig. 1 the dimensions of the modelled motion segment of the lower lumbar spine (L4-L5) are given. For the disc and vertebra the gross dimensions are in agreement with the anatomical data of Aharinejad et al. (1990), for the endplate Robert et al. (1989) is used. The chosen geometry and its dimensions are comparable with Shirazi-Adl (1989).

Six different tissue types are modelled: nucleus pulposus (NP), anulus fibrosus (AF), cartilaginous endplate (CEP), bony endplate (BEP), cancellous bone (CAB), and cortical bone (COB). The transverse areas of the nucleus and the anulus are equal. The outer anulus area equals also the latter areas. Both $z=0$ and the top are planes of symmetry. In fig. 1 the different areas and materials are depicted.
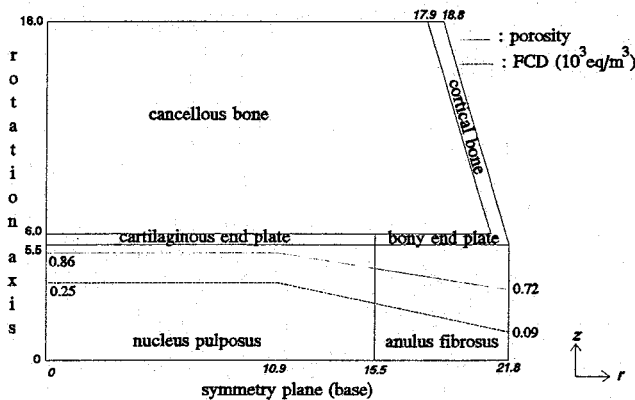

Fig. 1: The geometry and materials; the porosity (volume fraction of water) and the fixed charge density as a function of radial distance are given. The dimensions are in mm.

Material properties

The triphasic material behaviour of the tissue involves the stress-strain relation, the permeability, the porosity, the proteoglycan concentration or fixed charge density (FCD), and the osmotic coefficient. Only the 'soft' tissues are supposed to be osmotically active. The radial profile of the FCD across the nucleus and the anulus is given in fig. 1 (Urban and Maroudas, 1979). In the axial direction a homogenous distribution is assumed. The radial profile of the FCD in the CEP equals the one of the nucleus (Roberts et al., 1989). In the axial direction of the CEP the FCD decreases linearly to the value in the CAB: $0.001*10^3$ eq/m^3. The porosity profile of the soft tissues has the same shape as the FCD profile (Urban and Maroudas, 1979). For the cancellous bone a value of 0.5 is used. As the cortical bone and the bony endplate are dense materials a porosity of 0.01 is used. The osmotic coefficient is the same for all tissues and

equals 2.1 kPa/(m^{3}mol).

For all tissue types a linear relationship between the second Piola-Kirchhoff stress and the Green-Lagrange strain is assumed. The bi- and triphasic material properties are taken to be identical. The nucleus and the bony parts are isotropic. The Young's moduli and the Poisson's ratios are listed in table 1. The anulus fibrosus and the cartilaginous endplate are composed of a ground substance with imbedded collagen fibres. Both tissues are viewed upon as a homogenous mixture of matrix and fibres. Due to the orientation of the fibres the mixture has direction dependent properties. A perfect bond between the fibres and the matrix is assumed. The properties of the mixture are calculated according to the rules given by Hashin and Rosen (1964). The initial parameters needed are: the Young's modulus, Poisson's ratio, and the volume fraction of the fibres, the Young's modulus and the Poisson's ratio of the matrix. The Young's modulus and volume fraction of the fibres increase almost linearly in radial direction across the anulus. The volume fraction increases from 12.5% to 20.9% (Brickley-Parsons and Glimcher, 1983), the Young's modulus from 225 MPa to 595 MPa (Marchand and Ahmed, 1989). For the CEP values of 35% and 200 MPa are used. We found no experimental data for the Poisson's ratio of the fibres and assume a value of zero. A sensitivity analysis for fibre Poisson's ratios varying from 0 to 0.4 shows the following changes in the mixture (matrix + fibre) properties after rotation to model axes: maximal 0.3% in the Young's moduli and maximal 15% in the Poisson's ratios. The material constants are listed in table 1.

	Young's modulus	Poisson's ratio / fibre %	Permeability	Porosity	FCD[*]
	MPa	[-] / %	10^{-16} m^4/Ns	[-]	10^{+3} eq/m^3
NP	1.5	0.1/-	9.0	fig. 1	fig. 1
AF matrix inner fibres outer fibres	2.5 225 595	0.1/- 0.0/12.5 0.0/20.9	9.0	fig. 1	fig. 1
CEP matrix fibres	2.5 200	0.1/- 0.0/35.0	27.0	fig. 1	fig. 1
BEP	50	0.3/-	0.01	0.01	0.001
CAB	100	0.3/-	1000.0	0.01	0.001
COB	10000	0.3/-	0.01	0.5	0.001

Table 1: Material constants for a human lumbar motion segment. The F(ixed) C(harge) D(ensity) is defined as the number of equivalent (charge) moles per m^3 H$_2$O. [*]: the FCD is naturally used in the triphasic model only.

The fibres, arranged in lamellae, incline with respect to the transverse plane. The angle changes from $+\alpha$ to $-\alpha$ from one layer to the other. A value of 30 degrees is used for the anulus fibres, while an angle of 10 degrees is used for the cartilaginous endplate. With respect to a coordinate system aligned in the fibre direction a transverse isotropic stress-strain relation $SE(\alpha)$ is obtained.

Rotating this relationship to the global coordinate system yields a stress-strain relation with coupling between shear stresses and normal strains. By combining the contribution of a $+\alpha$ and a $-\alpha$ lamella according to SE = ½ (SE(α) + SE($-\alpha$)) the coupling terms vanish. The resulting stress-strain relation is orthotropic in the global coordinate system.

The simulation of an axial compression of the MS

The initial heights of the bi- and triphasic MS are taken to be identical. Because the triphasic MS has a swelling tendency, a preload has to be applied in order to keep its height identical to the biphasic height. The magnitude of this load is calculated by fixing the MS to the predetermined height, letting it swell until equilibrium is reached and calculating the axial force that is required to keep it in place. In addition to this preload the actual load is applied. In the biphasic case no preload is required and the simulation starts with the immediate load application.

The conditions at the time of application of the actual load are:

	biphasic	triphasic
fluid pressure	0 MPa	equals osmotic pressure
axial dimension	16 mm	16 mm
fibre stress	0 MPa	prestressed
preload	0 N	150 N

The boundary conditions are:

	biphasic	triphasic
pressure	0 MPa	equals osmotic pressure
displacements		
at the base	$u_z = 0$	$u_z = 0$

The axial displacements of the top nodes have been made identical by means of tyings. The load is 650 N for both the models. The COB and BEP are modeled impermeable. Hence, fluid flow is only possible through the NP, AF, CEP, and CAB.

Results

The results of the comparison between the bi- and triphasic models are given in the form of decrease in height of the top versus time, total integrated fluid flow versus time, fluid pressure and the fibre 2nd Piola Kirchhoff stresses in the anulus fibres.

In fig. 2 the decrease in height of the top over time is given. The biphasic height decrease is 16% more than in the triphasic case. Also, the triphasic simulation reaches equilibrium after 8 h, while the biphasic simulation does not even after 10 h. Total axial displacement is -1.055 mm in the triphasic simulation and -1.225 mm in the biphasic simulation.

Fluid can flow out of the IVD through the end plate and the anulus. Through the end plate the fluid flows into the cancellous bone and from there into the blood vessels that run in large numbers through the vertebra. Through the anulus fluid disappears into the interstitial spaces and can be absorbed by the surrounding tissues. Fig. 3a shows a qualitative picture of the fluid flow, whilst in fig. 3b the integrated flows are given. The total triphasic fluid loss is 28% smaller
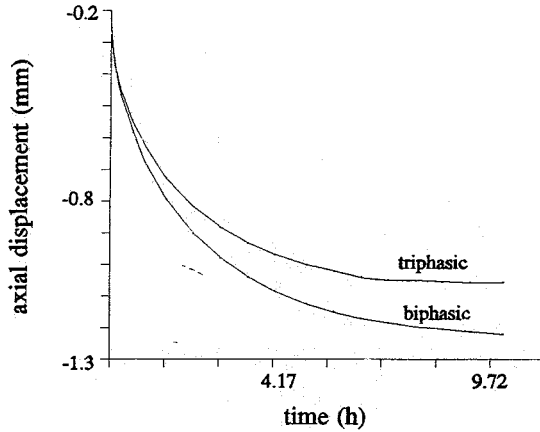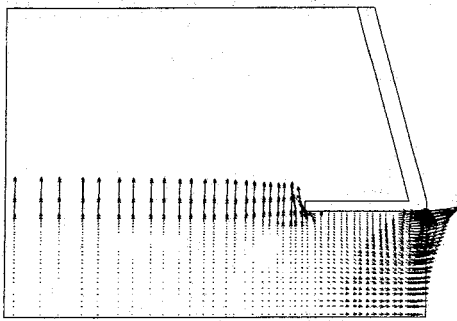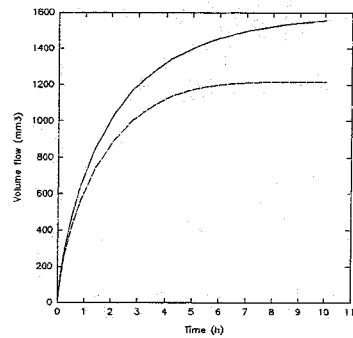
Fig. 2: The decrease in height versus time for bi- and triphasic motion segments

a.   b.

Fig. 3: a. Qualitative view of a fluid flow pattern through the MS. b. Integrated flow versus time; solid line: biphasic; dashed line: triphasic.

than the biphasic loss (1215 mm³ versus 1557 mm³).

The fluid pressure along the anulus base for t = 50 s and t = 10 h is given in fig. 4. The triphasic pressure is in both cases higher than the biphasic one. After 10 h the biphasic pressure has almost reduced to zero (< .01 MPa), while the triphasic pressure runs from 0.05 MPa (outermost anulus sheet) to 0.16 MPa (innermost anulus sheet). The maximum pressures in the nucleus are:

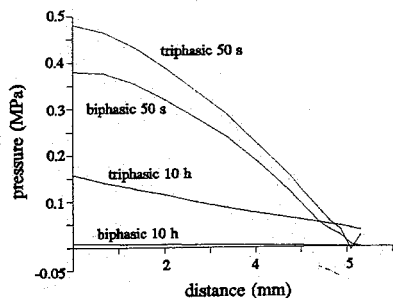|	biphasic	triphasic
initial	0 MPa	0.188 MPa
after 10 s	0.480 MPa	0.663 MPa
after 10 h	0.008 MPa	0.261 MPa

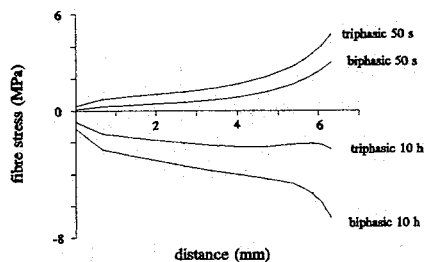**Fig. 4: Fluid pressure along the anulus base**

Fig. 5: The 2nd Piola Kirchhoff stress along the anulus base.

The fibre stress curves along the anulus base for different times are shown in fig. 5. Initially, (after 50 s) the fibre stresses are largest. They decrease in time and become negative ultimately. The triphasic stresses are higher than the biphasic stresses. After 50 s the triphasic stress at the base at the anulus edge is 60% higher than the biphasic stress (4.8 MPa versus 3 MPa).

Summarizing we find that in an axial compression simulation of the motion segment major differences occur in axial displacement (biphasic 16% more than triphasic), expelled fluid volume versus time (after 10 h triphasic 28% less), fluid pressure (at the base at the inner anulus after 50 s triphasic 26% higher than biphasic), and fibre stress (at the base at the anulus edge after 50 s triphasic 60% higher than biphasic). Although the triphasic simulation maintains a higher fluid pressure, less water is expelled.

Conclusions and discussion

This study is to our knowledge the first to present a triphasic finite element model of the intervertebral disc. The comparison of biphasic and triphasic simulations shows that (1) the triphasic model holds on to more water although the triphasic fluid pressure gradients are larger and (2) the anulus tensile fibre stresses are larger in the triphasic computation compared to the biphasic computation. The triphasic simulation loses less height (3) and reaches equilibrium earlier (4).

In comparing the two models it is important to be aware of some fundamental differences between them. In both models it is possible for the structures to attract water. The mechanisms by which this occurs are completely different. In the biphasic model fluid can be imbibed because of the elasticity of the tissue. In the triphasic case the attraction of fluid molecules has its origin in the osmotic effect and the elasticity of the tissue. Because the osmotic force is deformation

dependent through the dependency on the FCD, the biphasic model cannot be simply adjusted by adding a simple term to the biphasic stiffness (to compensate for the osmotic stiffness). A triphasic model is needed.

Berkson et al. (1979) measured fluid pressures in the nucleus in axial compression experiments. They found that the nucleus pressure was 1.22 (compression load 400 N) to 1.99 (compression load 100 N) times the outer applied load per unit surface of the IVD (the facet joints excised). For the triphasic simulation this factor (P) is 1.87 initially (with the preload of 150 N). In the loading stage shortly (10 s) after application of the load it is 1.24, and after 10 h it equals 1.10. In the biphasic experiment the values after 10 s and 10 h are, respectively, 0.49 and 0.018.

There are three important conclusions to be drawn from these data: (1) The factor P depends on the external load (experiment+simulation), (2) P is dependent on time (simulation), and (3) P is greater than one in the triphasic case and in the experiment, whilst it is smaller than one for the biphasic computation. This means that the biphasic maximum nucleus pressure is smaller than the outer load per unit area of IVD. The reverse is true for the triphasic computation and the experiments. There is good agreement between the triphasic simulation and the experiment. One should bear in mind that the values of P reported by Berkson et al. are based on in vitro measurements with 100 percent relative humidity conditions, and our simulations are done in a salt solution with constant concentration. The values should be compared shortly after application of the load ($<$ 15 min) at which time the measurements in vitro have been performed.

Although the triphasic fluid pressure is higher (fig. 4), less water is expelled (fig. 3b). In short: the triphasic material holds on to more water at higher pressures. This effect can be understood when we consider that the driving force for fluid flow is the combined effect of concentration gradients and pressure gradients (the continuity equation (1.2)).

The triphasic fibre stress is seen to be higher at all points in time, as is shown in fig. 5 for t = 50 s and t = 10 h. The triphasic model would predict earlier breakage of fibres than would the biphasic model. In time, the fibre stresses decrease uniformly. This means that fibre breakage in this modelling situation is most likely to occur directly after application of the load. It should be noted that the fibre angle also determines the value of the stress (through rotation of the stresses in the model axes), while the measured values show a wide range (variation by as much as 35°), even in one individual fibre sheet (Marchand and Ahmed, 1990). By choosing a smaller angle (than 30°) the stresses will increase. Tensile Cauchy stress at failure of anulus specimens cut along the fibre direction was found to be 8.8 ± 1.1 MPa (n=18; Galante, 1967).

The comparison of radial deformation with experimental data is complicated because of the influence of the preload (Panjabi and Krag, 1977), and the time dependence of the axial deformation (fig. 2). Panjabi and Krag found significant differences in radial deformation using 3 different preloads: 0, 400 and 1000 N and very small additional loads: up to 150 N. The axial deformation at a load of 150 N with the different preloads lay in the range of -0.01 to -0.02 mm. They also concluded that the effect of preload may be different for different physiological loads. Their findings make it difficult for us to compare the numerical results with 150 N preload and 650 N additional load with experimen-

tal results without preload. Hirsch and Nachemson (1954) found a mean axial displacement of -0.75 mm (n=94; -1.5 mm for the whole motion segment; our axial displacement data are based on half of the MS) with a load of 1000 N. This is smaller than our predicted values after 10 h. However, they measured after a relatively short time (minutes) after the application of the load, while we find at that point in time significant creep response in our simulation. Therefore, we only give these results to get an indication of the order of magnitude.

Berkson et al. (1979) measured no-load intradiscal pressures and found a mean value of 0.076 MPa (n=42) with the posterior elements (facet joints) destroyed. In unloaded biphasic material in which the pores are in open contact with a fluid environment, the pore pressure necessarily goes to the pressure of the environment. We did not model the unloaded situation, but in the preload equilibrium situation the nucleus pressure ranges from 0.11 MPa to 0.19 MPa. These values may be comparable with the experimental data of Berkson et al., keeping in mind that the 150 N preload has a P factor of 1.9 for the pressure of 0.19 MPa and 1.1 for 0.11 MPa.

References

Adams, M.A., Hutton, W.C. The effect of posture on the role of the apophysial joints in resisting intervertebral compressive forces. J. Bone Joint Surg. [Br], 62B:358-362, 1980

Aharinejad, S., Bertagnoli, R., Wicke, K., Firbas, W., Schneider, B. Morphometric analysis of vertebrae and intervertebral discs as a basis of disc replacement. Am. J. Anat., 189:69:76, 1990.

Berkson, M.H., Nachemson, A., Schultz, A.B. Mechanical properties of human lumbar spine motion segments-Part 2: responses in compression and shear; influence of gross morphology. Journal of Biomechanical Engineering, 101:53-57, 1979

Bowen, R.M. Incompressible porous media models by use of the theory of mixtures. Int. J. Eng. Sci., Vol 18, 1129-1148, 1980

Brickley-Parsons, D., Glimcher, M.J. Is the chemistry of collagen in intervertebral discs an expression of Wolff's law? A study of the human lumbar spine. Spine, 9,2:148-163, 1984.

Galante, J.O. Tensile properties of the human lumbar annulus fibrosis. Acta Orthopedica Scandinavica Suppl. 100:1:5-91, 1967

Hashin, Z., Rosen, B.W. The elastic moduli of fiber-reinforced materials. J. Appl. Mech., 223-230, 1964

Hirsh, C., Nachemson, A. A new observation on the mechanical behaviour of lumbar discs. Acta Orthop. Scan., 23:254-283, 1954

Lai, W.M., Hou, J.S., Mow, V.C. A triphasic theory for the swelling and deformation behaviors of articular cartilage. J. of Biomech. Engng., 113:245-258, 1991

Marchand, F., Ahmed, A.M. Mechanical properties and failure mechanism of the constituent components of annulus fibrosus. Proc. 10th Annu. CBS, Montreal, Quebec, 1989.

Müller, I. Thermodynamics. Pitman Advanced Publishing Program, Boston, 1-202, 1985.

Panjabi, M.M, Krag, M.H. Effects of preload on load displacement curves of the lumbar spine. Orthopedic Clinics of North America, 8:181-192, 1977

330

Roberts, S., Menage, J., Urban, J.P.G. Biochemical and structural properties of the cartilage end-plate and its relation to the intervertebral disc. Spine, 14:166-174, 1989.

Shirazi-Adl, A. On the fibre composite material models of disc annulus-comparison of predicted stresses. J. Biomech., 22:357-365, 1989.

Simon, B.R., Wu, J.S.S., Carlton, M.W., Evans, J.H., Kazarian, L.E. Structural models for human spinal motion segments based on a poroelastic view of the intervertebral disk. J. Biomech. Engng., 107;327-335, 1985.

Snijders, H., Huyghe, J., Willems, P., Drost, M., Janssen, J., Huson, A. A mixture approach to the mechanics of the human intervertebral disc. in: Mechanics of swelling: from clays to living cells and tissues, ed. T.D. Karalis, 1992.

Snijders, H., Huyghe, J.M., Drost, M.R., Willems, P., Janssen, J.D., Huson A. Triphasic finite element model for intervertebral disc tissue. in: Computer Methods in Biomechanics and Biomedical Engineering Symposium, Middleton, J., Pande, G.N., Williams, K.R. (eds), in press

Urban, J., Maroudas, A. The measurement of fixed charge density in the intervertebral disc. Biochimica et Biophysica Acta, 586:166-18, 1979.